Research in
Astronomy and
Astrophysics

Charge transfer and excitation processes in low energy collisions of He$^+$ ions with Li atoms

Xiao-Xia Wang[1], Kun Wang[2], Yi-Geng Peng[3], Chun-Hua Liu[4], Ling Liu[5], Yong Wu[5], Heinz-Peter Liebermann[6], Robert J. Buenker[6] and Yi-Zhi Qu[1]

[1] College of Material Sciences and Optoelectronic Technology, University of Chinese Academy of Sciences, Beijing 100049, China; *yzqu@ucas.ac.cn*

[2] Institute of Environmental Science, Shanxi University, Taiyuan 030006, China

[3] Department of Applied Physics, Nanjing University of Science and Technology, Nanjing 210094, China

[4] School of Physics, Southeast University, Nanjing 210094, China

[5] Data Center for High Energy Density Physics, Institute of Applied Physics and Computational Mathematics, Beijing 100088, China

[6] Fachbereich C-Mathematik und Naturwissenschaften, Bergische Universitat Wuppertal, D-42097 Wuppertal, Germany

Abstract Electron capture between solar wind ions and neutral species has contributed to the understanding of X-ray production from solar system bodies. The charge transfer and excitation processes in solar wind ions of He$^+(1s)$ colliding with Li$(1s^2 2s)$ atoms are studied by utilizing the full quantum-mechanical molecular-orbital close-coupling (QMOCC) method with impact energies of 0.003–2 keV amu^{-1}. Comparisons of cross sections from single- and multi-configurational calculations for a self-consistent field (SCF and MCSCF) process are carried out. Results show that the dominant reaction channels are He$(1s2l\ ^{1,3}\mathrm{L})$ + Li$^+(1s^2\ ^1\mathrm{S})$. Good consistency is found among present total and state-selective charge transfer and excitation cross sections with other theoretical and experimental data in the same energy region. Due to the differences between coupling matrix elements in high-energy states, the charge transfer cross sections calculated from SCF and MCSCF split slightly as $E > 0.4$ keV amu^{-1}. Weak Stueckelberg oscillations for charge transfer appear in the present work. In addition, the differences of cross sections for electron excitation to Li$(1s^2 2p)$ in the singlet/triplet molecular states with He$^+(1s)$ are much smaller than those of charge transfer processes because of the similar energy gaps from Li$(1s^2 2p)$ to the ground state in singlet/triplet states in the large R region.

Key words: Sun: solar wind — ISM: molecules — ISM: kinematics and dynamics — molecular processes

1 INTRODUCTION

The study of charge transfer processes by ions colliding with atoms or molecules is significant in astrophysical and man-made plasmas (Lubinski et al. 2001). These processes can change the distributions of charge and electronic state, and influence the ionization balance and radiation losses (Dalgarno 1985). In particular, they have important applications in astrophysics researches (Isler 1994). In an astronomy environment, the charge transfer has been confirmed as a major cause of the soft X-ray background (SXRB) (Cravens 2000; Krasnopolsky & Mumma 2001; Bhardwaj et al. 2006, 2007), which is produced in solar wind ions colliding with neutral gases in comets, and solar

and stellar atmospheres, namely the solar wind charge exchange (SWCX) process (Lin et al. 2019).

The solar wind originates from activity in the solar corona and is composed of electrons, protons, He^{2+} ions and a small fraction of highly ionized heavier ions. As reported by Swaczyna et al. (2019), after charge exchange with interstellar neutral atoms a number of solar wind He^{2+} turn into He$^+$, which become an important constituent of the solar wind. Lithium atoms which originated in the Big Bang are one of the most abundant elements in the universe after hydrogen and helium (Polosukhina et al. 2010; Polosukhina & Shavrina 2007; Ramírez et al. 2012). Furthermore, collisions of multiply charged ions with lithium atoms can also be

used to diagnose the property of plasmas in thermonuclear fusion reactors by means of Li beam spectroscopy (Schweinzer et al. 1994).

Because of the suggested applicability above and the quasi-one-electron models of the element Li in theoretical descriptions, there are many earlier studies of the charge exchange process for He$^+$ colliding with Li in a large energy region. Aucicllo et al. (1976) and McCullough et al. (1982) measured the charge transfer cross sections of He$^+$ colliding with Li in the energy range of 5–44 keV (1.25–11 keV amu^{-1}) and 6.7–800 keV (1.68–200 keV amu^{-1}). Varghese et al. (1984) reported the experimental cross sections at projectile energies between 0.257 and 8.2 keV (0.06–2.05 keV amu^{-1}). Later, Aumayr & Winter (1985b) and Dubois & Toburen (1985) measured the cross sections at impact energies of 2–20 keV (0.5–5.0 keV amu^{-1}) and 2–100 keV(0.5–25 keV amu^{-1}), respectively. As far as we know, the first theoretical results appeared in Bransden et al. (1984) relying on a two-center atomic orbital expansion between 1 and 400 keV (0.25–100 keV amu^{-1}). Liu et al. (2016) studied the electron capture from Li by He$^+$ applying the two-center atomic orbital close-coupling (TC-AOCC) method in a wide energy range of 0.1–100 keV amu^{-1}. The experimental and theoretical results seem to be in general agreement in the whole energy range, except that when the collision energies $E > 0.5$ keV amu^{-1}, the total charge transfer cross sections calculated by Bransden et al. (1984) are closer to the measurements of Aumayr & Winter (1985b). However, the TC-AOCC results of Liu et al. (2016) agree well with the experimental data of Varghese et al. (1984) and Dubois & Toburen (1985), which are about 20%–50% larger than those of Aumayr & Winter (1985b). It is convenient to classify the available data between 0.5 and 5 keV amu^{-1} into two groups based on the values of total charge transfer cross sections. Results of Aumayr & Winter (1985b) and Bransden et al. (1984) are included in the low group (LG), while the high group (HG) is comprised of data from Varghese et al. (1984), Dubois & Toburen (1985) and Liu et al. (2016). Discrepancies exist among experimental and theoretical works in the impact energies of 0.5–5 keV amu^{-1}. In addition, few studies have appeared below the energies of 0.1 keV amu^{-1}. More investigations are expected for the He$^+$ and Li collision system.

In this paper, the charge transfer and excitation processes caused by the He$^+$ ion impact on Li atoms in the energy region of 0.003 to 2 keV amu^{-1} are investigated by relying on the quantum-mechanical molecular-orbital close-coupling (QMOCC) method (Bransden & McDowell 1992; Zygelman et al. 1992). In order to test the convergence of our calculations,

two sets of orbitals are considered, i.e., the single- and multi-configurational self-consistent field (SCF and MCSCF respectively (Werner & Knowles 1985; Knowles & Werner 1985)) methods are performed by utilizing the multi-reference single- and double-excitation configuration interaction (MRDCI) package (Buenker & Phillips 1985; Krebs & Buenker 1995) and the MOLPRO (Hans-Joachim et al. 2010) program, respectively. Then by adopting these two orbital sets into the MRDCI package for the following CI procedures, the potential energy curves, and radial and rotational coupling matrices are obtained. Comparisons between the present charge transfer/excitation cross sections and the existing experimental and theoretical data are presented. Atomic units are used throughout unless otherwise stated.

2　THEORETICAL METHODS

2.1　Scattering Calculations

The nonradiative charge transfer/excitation cross sections for He$^+$ colliding with Li have been calculated by employing the QMOCC method. A brief description of this method is given here as more details have been provided elsewhere (Kimura & Lane 1989; Zygelman et al. 1992). In the perturbed stationary state (PSS) model (Heil et al. 1981; Bransden & McDowell 1992; Zygelman et al. 1992), the total wave functions of a collision system can be expanded approximately in terms of the adiabatic electric wave function $\psi_i(\overrightarrow{R}, \overrightarrow{r})$

$$\Psi(\overrightarrow{R}, \overrightarrow{r}) = \sum_i F_i(\overrightarrow{R})\psi_i(\overrightarrow{R}, \overrightarrow{r}). \qquad (1)$$

Here $\overrightarrow{R}$ and $\overrightarrow{r}$ are the internuclear distance and electron position vector in the center of mass coordinate of nuclei. After partial wave expansion for each channel function $F_i(\overrightarrow{R})$, the radial function $f^J(R)$ satisfies this differential equation in rotating coordinates

$$\left[\frac{d^2}{dR^2} - \frac{J(J+1) - \lambda^2}{R^2} - 2\mu(u(R) - E)\right] f^J(R)$$
$$= (V^R(R) + V^C(R))f^J(R). \qquad (2)$$

Here μ and u are the reduced mass and the diagonal adiabatic potential matrix respectively. $J(J+1)$ and λ are eigenvalues of the total angular momentum $\overrightarrow{J}^2$ and the electronic angular momentum L_z, respectively. V^R and V^C are matrices of the radial and rotational coupling, which connect the adiabatic states and cause transition between the same (V^R) or different (V^C) symmetry. The most important term in radial coupling can be expressed as $A^R_{ij} = \langle i| \frac{\partial}{\partial R} |j\rangle$, which is usually calculated by finite-difference methods. But as A^R_{ij} is nearly singular and

Table 1 Asymptotic Atomic Energies for the HeLi$^+$ Molecular States to the Singlet States

Molecular states	Asymptotic atomic states	Energy and error (eV)		
		NIST(Kramida et al. 2019)	MRDCI	Error
$1^1\Sigma^+$	He($1s^2$ ^{1}S) + Li$^+$($1s^2$ ^{1}S)	-19.196	–19.182	0.014
$2^1\Sigma^+$	**He$^+$($1s$ ^{2}S) + Li($1s^2 2s$ ^{2}S)**	**0**	**0**	**0**
$3^1\Sigma^+$	He($1s2s$ ^{1}S) + Li$^+$($1s^2$ ^{1}S)	1.420	1.416	-0.004
$4^1\Sigma^+, 1^1\Pi$	He$^+$($1s$ ^{2}S) + Li($1s^2 2p$ ^{2}P^o)	1.847	1.838	-0.009
$5^1\Sigma^+, 2^1\Pi$	He($1s2p$ ^{1}P^o) + Li$^+$($1s^2$ ^{1}S)	2.022	2.017	-0.005
$6^1\Sigma^+$	He$^+$($1s$ ^{2}S) + Li($1s^2 3s$ ^{2}S)	3.373	3.362	–0.011
$7^1\Sigma^+$	He($1s3s$ ^{1}S) + Li$^+$($1s^2$ ^{1}S)	3.724	3.755	0.031
$8^1\Sigma^+, 3^1\Pi$	He$^+$($1s$ ^{2}S) + Li($1s^2 3p$ ^{2}P^o)	3.834	3.816	–0.018
$9^1\Sigma^+, 4^1\Pi$	He($1s3p$ ^{1}P^o) + Li$^+$($1s^2$ ^{1}S)	3.891	3.888	–0.003
$10^1\Sigma^+, 5^1\Pi, 1^1\Delta$	He$^+$($1s$ ^{2}S) + Li($1s^2 3d$ ^{2}D)	3.878	3.899	0.021
$11^1\Sigma^+, 6^1\Pi, 2^1\Delta$	He($1s3d$ ^{1}D) + Li$^+$($1s^2$ ^{1}S)	3.878	3.905	0.027

Table 2 Asymptotic Atomic Energies for the HeLi$^+$ Molecular States to the Triplet States

Molecular states	Asymptotic atomic states	Energy and error (eV)		
		NIST(Kramida et al. 2019)	MRDCI	Error
$1^3\Sigma^+$	**He$^+$($1s$ ^{2}S) + Li($1s^2 2s$ ^{2}S)**	**0**	**0**	**0**
$2^3\Sigma^+$	He($1s2s$ ^{3}S) + Li$^+$($1s^2$ ^{1}S)	0.624	0.608	–0.016
$3^3\Sigma^+, 1^3\Pi$	He($1s2p$ ^{3}P^o) + Li$^+$($1s^2$ ^{1}S)	1.768	1.758	–0.010
$4^3\Sigma^+, 2^3\Pi$	He$^+$($1s$ ^{2}S) + Li($1s^2 2p$ ^{2}P^o)	1.847	1.835	–0.012
$5^3\Sigma^+$	He$^+$($1s$ ^{2}S) + Li($1s^2 3s$ ^{2}S)	3.373	3.362	–0.011
$6^3\Sigma^+$	He($1s3s$ ^{3}S) + Li$^+$($1s^2$ ^{1}S)	3.522	3.537	0.015
$7^3\Sigma^+, 3^3\Pi$	He($1s3p$ ^{3}P^o) + Li$^+$($1s^2$ ^{1}S)	3.811	3.807	–0.004
$8^3\Sigma^+, 4^3\Pi$	He$^+$($1s$ ^{2}S) + Li($1s^2 3p$ ^{2}P^o)	3.834	3.816	-0.018
$9^3\Sigma^+, 5^3\Pi, 1^3\Delta$	He($1s3d$ ^{3}D) + Li$^+$($1s^2$ ^{1}S)	3.878	3.892	0.014
$10^3\Sigma^+, 6^3\Pi, 2^3\Delta$	He$^+$($1s$ ^{2}S) + Li($1s^2 3d$ ^{2}D)	3.878	3.892	0.014

changes very rapidly near an avoided crossing, generally a unitary transformation is made to transform the adiabatic representation to a diabatic one, in which the A_{ij}^R is smoothly varying or zero. Under this transformation, the radial function relates to

$$f^J(R) = Cg^J(R),$$
$$\frac{dC}{dR} + AC = 0. \tag{3}$$

C is the unitary transformation matrix when $R \rightarrow \infty$ and $C(R) \rightarrow \overleftrightarrow{I}$. Correspondingly, the radial coupling function becomes

$$\left[\frac{d^2}{dR^2} - \frac{J(J+1)-\lambda^2}{R^2} + 2\mu E\right] g_\gamma^J - 2\mu \sum_{\gamma'} U_{\gamma,\gamma'}(R)g_{\gamma'}^J = 0,$$
$$U_{\gamma,\gamma'}(R) \equiv [C(u-P)C^{-1}]_{\gamma\gamma'}. \tag{4}$$

$U(R)$ is the diabatic potential matrix whose off-diagonal elements contribute to the charge transformation. P is the rotational coupling matrix with elements

$$P_{ij} = \mp\frac{1}{\mu R^2}[(J \mp \lambda_i)(J \pm \lambda_i + 1)]^{1/2} A_{ij}^\theta \delta(\lambda_i, \lambda_j \mp 1)]. \tag{5}$$

To solve Equation (4) the multichannel log-derivative algorithm of Johnson (1973) is implemented, from which the K matrix is obtained. The S matrix can be written as

$$S_J = \frac{I + iK_J}{I - iK_J}. \tag{6}$$

The cross section for states i to j can be defined as

$$\sigma_{(i \rightarrow j)} = \frac{\pi}{k_i^2} \sum_J (2J+1) |S_J|_{i,j}^2. \tag{7}$$

Although the PSS model is reliable for very low energies, it has inherent defects such as the individual terms in the expansion (1) do not satisfy the scattering boundary conditions. At moderate impact velocities, these defects can be corrected by introducing the Bate-McCarroll plane-wave translation factors (Bransden & McDowell 1992) and the total wave functions are expressed by

$$\Psi(\overrightarrow{R}, \overrightarrow{r}) = \sum_i F_i(\overrightarrow{R})\psi_i(\overrightarrow{R}, \overrightarrow{r}) \exp(i\gamma(\overrightarrow{R}, \overrightarrow{r})). \tag{8}$$

$\exp(i\gamma(\overrightarrow{R}, \overrightarrow{r}))$ is electron translation factor (ETF). By choosing the reaction coordinates and switching function from Gargaud et al. (1987), which is identical to the semi-classical common translation factor (CTF) adopted by Errea et al. (1982), the radial and rotational interaction can be replaced by (Bacchus-Montabonel & Ceyzeriat 1998)

$$\langle i|\partial/\partial R - (\varepsilon_i - \varepsilon_j)z^2/2R|j\rangle,$$
$$\langle i|iL_y + (\varepsilon_i - \varepsilon_j)zx|j\rangle, \tag{9}$$

where z^2 and zx are the components of the quadrupole moment tensor, and ε_i and ε_j are the electronic energies of states ψ_i and ψ_j respectively.
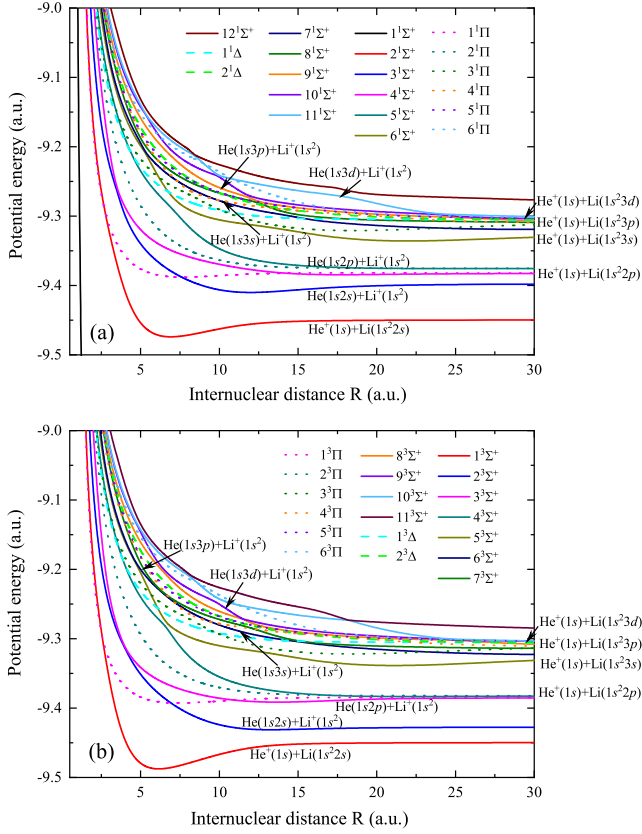
Fig. 1 Adiabatic potential curves for HeLi$^+$ molecular states in singlet (a) and triplet (b) manifolds. The solid, dotted and dashed lines represent the Σ^+, Π and Δ states, respectively.

2.2 Electronic Structure Calculations

The electronic structures of the HeLi$^+$ system are obtained from the *ab initio* configuration-interactions (CIs) method (Lischka et al. 2018). For the choice of basis set, the Aug-cc-pVQZ (augmented correlation consistent polarization valence quadruple ζ) basis set is employed, i.e. the $(13s,7p,4d)$ basis set contracted to the $[6s,5p,4d]$ is used for lithium and the $(8s,4p,3d)$ contract to $[5s,4p,3d]$ for helium. The f and g Gaussian-type functions are deleted for hardly influencing the precision of the electronic structures. In order to describe the Rydberg states of the He atom well, a diffuse $(2s, 2p, 2d)$ basis of He is added. The spin-orbit interactions are not considered because of the slight fine-structure splittings.

In the CI method, the wave functions ψ_n of electron state n can be expanded approximately by finite determinant wave functions or configuration state functions Φ_i

$$\psi_n = \sum_i c_i^n \Phi_i, \qquad (10)$$

in which $\{c_i^n\}$ are the linear expansion coefficients with $\sum_i \left(c_i^n\right)^2 = 1$ and $\langle \Phi_i | \Phi_j \rangle = \delta_{ij}$. In traditional

SCF calculation, only the molecular orbitals in ground configuration Φ_0 are varied to obtain the minimal energy, while in the MCSCF calculations (Werner & Knowles 1985; Knowles & Werner 1985) both the CI coefficients $\{c_i^n\}$ and molecular orbitals, from which the configurations Φ_i are constructed, are varied. In our calculation, the SCF and MCSCF processes are performed by the MRDCI and MOLPRO (Hans-Joachim et al. 2010) programs, respectively, then the orbital sets are adopted into the MRDCI treatment to perform the following CI calculations.

3 RESULTS AND DISCUSSION

3.1 Adiabatic Potentials and Couplings

The adiabatic potential energies of the HeLi$^+$ system have been calculated by the *ab initio* MRDCI package from internuclear distance $R = 1.0$ to 50.0 a.u. with a threshold of 5×10^{-8} hartree (1.36×10^{-6} eV) for configuration selection. For the collision of He$^+(1s)$ + Li$(1s^2 2s)$, eleven $^1\Sigma^+$ (ten $^3\Sigma^+$) and two $^1\Delta$ (two $^3\Delta$) states in A_1 symmetry as well as six $^1\Pi$ (six $^3\Pi$) states in B_1 symmetry corresponding to the charge-transfer/excitation states are included in the singlet (triplet) manifolds. Tables 1 and 2 list the energy levels for the HeLi$^+$ asymptotic atomic states of singlet/triplet manifolds (only MCSCF results are listed, as the differences between SCF and MCSCF calculation are about 10^{-3} a.u.) and compared with the experimental atomic energies from National Institute of Standards and Technology (NIST) (Kramida et al. 2019). The $2^1\Sigma^+$ and $1^3\Sigma^+$ states (shown in boldface) asymptotically corresponding to the He$^+(1s)$ + Li$(1s^2 2s)$ atomic state denote the initial channel in the singlet and triplet manifolds, respectively. The differences between our calculations and the experimental results are below 0.032 eV in the asymptotic region, which is sufficient for the following scattering calculations (Herrero et al. 1996).

The charge transfer and excitation channels are included in the adiabatic potentials of HeLi$^+$ molecular states. With the exception of the lowest [He$(1s^2)$ + Li$^+(1s^2)$; $1^1\Sigma^+$] in the singlet state, the Σ^+, Π and Δ states of the singlet/triplet manifolds in our calculations are entirely displayed in Figure 1(a) and (b) for internuclear distance from 1.0 to 30.0 a.u. Similarly, the MCSCF data are plotted due to the differences in 10^{-3} a.u. between SCF and MCSCF calculation. The lowest singlet state [He$(1s^2)$ + Li$^+(1s^2)$; $1^1\Sigma^+$] is about 19.20 eV lower than the entrance channel in asymptotical region, whose charge transfer processes should be insignificant. For the internuclear distance $R > 5$ a.u., the potential curves of the low-energy states show no obvious avoided crossings. Instance states [He$(1s2s)$ + Li$^+$; $3^1\Sigma^+/2^3\Sigma^+$] are closest
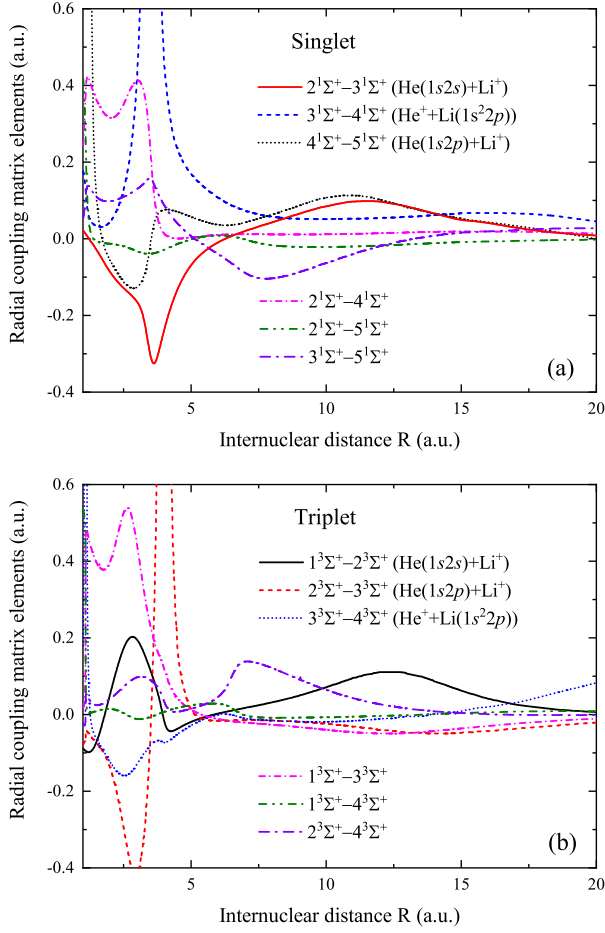
Fig. 2 Radial coupling matrix element among Σ^+ states for HeLi$^+$ molecular states. (a) singlet states; (b) triplet states.

Fig. 3 Rotational coupling matrix element among Σ^+ and Π states for HeLi$^+$ molecular states. (a) singlet states; (b) triplet states.

to the initial channels [He$^+$ + Li($1s^22s$); $2^1\Sigma^+/1^3\Sigma^+$], but no strong interactions are exhibited between them. It suggests that the charge transfer process between [He($1s2s$) + Li$^+$; $3^1\Sigma^+/2^3\Sigma^+$] and initial channels are driven by the Demkov-type mechanism (Kimura & Lane 1990; Liu et al. 2010), as well as between [He$^+$ + Li($1s^22p$); $4^1\Sigma^+/4^3\Sigma^+$], [He($1s2p$) + Li$^+$; $5^1\Sigma^+/3^3\Sigma^+$], etc. Avoided crossings appear between [He($1s2s$) + Li$^+$; $3^1\Sigma^+/2^3\Sigma^+$] and [He$^+$ + Li($1s^22p$); $4^1\Sigma^+/3^3\Sigma^+$] states at about 4.0 a.u., as well as between [He($1s2p$) + Li$^+$; $5^1\Sigma^+/4^3\Sigma^+$] and [He$^+$ + Li($1s^23s$); $6^1\Sigma^+/5^3\Sigma^+$] states $\sim$ 7.0 a.u. With the reduction of internuclear distances, the potential curves of the [He$^+$+ Li($1s^22p$); $1^1\Pi$] and [He($1s2p$) + Li$^+$; $1^3\Pi$] begin to approach the initial channels [He$^+$ + Li($1s^22s$); $2^1\Sigma^+/1^3\Sigma^+$], and then become degenerate around 2.5 a.u. As the energy increases, charge transfer and excitation channels appear alternately, which indicates that the electron excitation states may play an important part in He$^+$($1s$) + Li($1s^22s$) collisions.
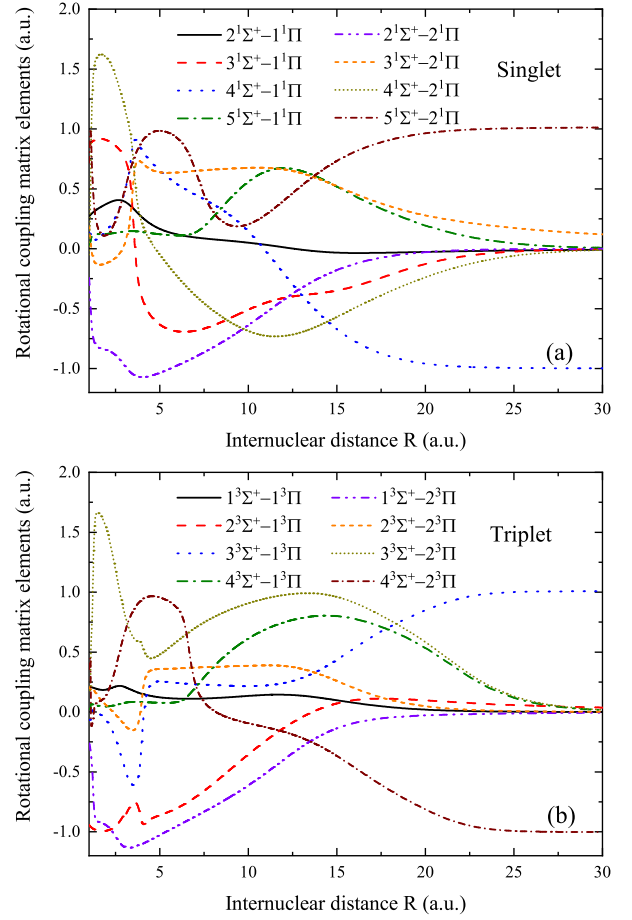
In low energy collisions, charge transfer processes mainly occur among states adjacent to the initial state, and the important matrix elements for radial and rotational couplings in the He$^+$($1s$)-Li($1s^22s$) system are mainly among the low-energy states. It is found that the coupling matrix elements of two low-energy states calculated by SCF and MCSCF almost coincide with each other, e.g. $2^1\Sigma^+$-$3^1\Sigma^+$, $2^3\Sigma^+$-$4^3\Sigma^+$ and $1^3\Sigma^+$-$1^3\Pi$. Their differences will be discussed later. Results from MCSCF calculations are displayed in Figures 2 and 3 with the ETF effects (Errea et al. 1982) included.

It is apparent in Figure 2 that except for the strong interactions between [He($1s2s$) + Li$^+$; $3^1\Sigma^+/2^3\Sigma^+$] and [He$^+$ + Li($1s^22p$); $4^1\Sigma^+/3^3\Sigma^+$] around 3.5 and 4.0 a.u., the radial couplings between the low-energy states are very weak. The usual shapes of the coupling matrix elements and the distinctive long-range interactions typically belong to Demkov-type coupling. As mentioned above, the [He($1s2s$) + Li$^+$; $3^1\Sigma^+/2^3\Sigma^+$] states are closest to the initial channels [He$^+$ + Li($1s^22s$); $2^1\Sigma^+/1^3\Sigma^+$], and broad and shallow peaks appear in their radial
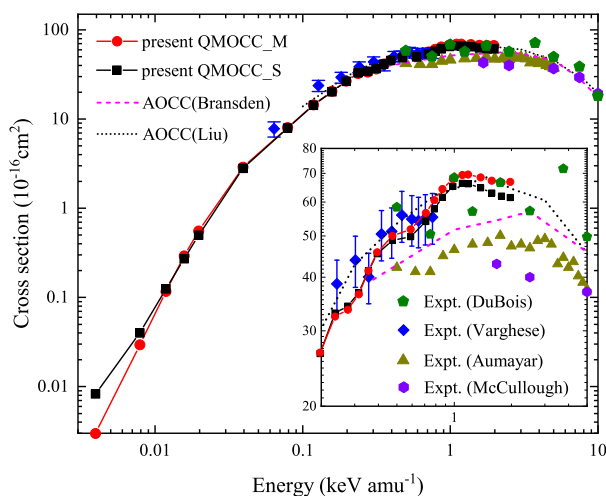
Fig. 4 Spin-average total charge transfer cross sections in He$^+$-Li collisions and comparison with other results as a function of collision energies. Theory: present QMOCC_M (*solid line with filled circles*) and QMOCC_S (*solid line with filled squares*), AOCC results of Liu et al. (2016) (*dotted line*), AOCC results of Bransden et al. (1984) (*dashed line*); experiment: Varghese et al. (1984) (*filled diamonds*), Aumayr & Winter (1985b) (*filled triangles*), Dubois & Toburen (1985) (*filled pentagons*) and McCullough et al. (1982) (*filled hexagons*).
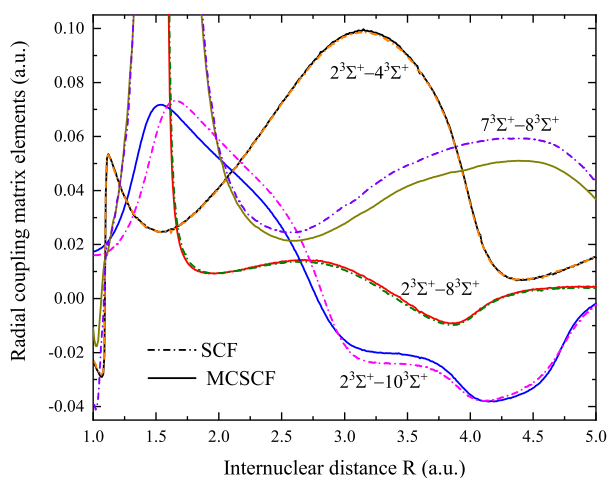
Fig. 5 Comparing examples of radial coupling matrix elements from SCF (*dash-dotted lines*) and MCSCF (*solid lines*) calculation.

couplings near 12.0 a.u. This signifies that the electron would dominantly transfer to the He($1s2s$) and these two couplings are the main gateway of charge-transfer flux from initial channel to the exit channels.

Electrons can also be captured by the Π states through the rotational couplings. As shown in Figure 3, the matrix elements of rotational couplings for the singlet manifolds are also formally similar to those for the triplet. For $R > 5$ a.u., compared with interactions between [He$^+$ + Li($1s^22s$); $1^3\Sigma^+$] and [He($1s2p$) + Li$^+$; $1^3\Pi$], the

rotational couplings between [He$^+$ + Li($1s^22s$); $2^1\Sigma^+$] and [He$^+$ + Li($1s^22p$); $1^1\Pi$] are much shallower, but it is the opposite in regions of $R < 5$ a.u. The probabilities of electron capture to the $1^3\Pi$ state may be larger than those to the $1^1\Pi$ state in low energy collisions. In addition, unlike the $1^3\Sigma^+$-$1^3\Pi$ coupling contributing to the charge transfer channel He($1s2p$) + Li$^+$, the $2^1\Sigma^+$-$1^1\Pi$ is responsible for the population of electron excitation channel He$^+$ + Li($1s^22p$).

3.2 Charge Transfer Cross Sections

3.2.1 Total cross sections

Based on the above analyses for the electronic structure of the HeLi$^+$ quasimolecule, the charge transfer cross sections for singlet/triplet states are calculated by the QMOCC method in impact energies between 0.003 and 2 keV amu^{-1}. The present total charge transfer cross sections acquired from spin-averaged total charge transfer cross sections of singlet (25%) and triplet (75%) manifolds are displayed in Figure 4 (Supplemental materials: Table S1). Results of SCF and MCSCF calculations are labeled by QMOCC_S and QMOCC_M, respectively. The potential energies and coupling matrix elements between two low-energy states of HeLi$^+$ calculated by SCF and MCSCF nearly coincide with each other. However, it is the slight differences of coupling matrix elements in high-energy states calculated by these two methods whose contribution to cross sections increases with increasing impact energy that lead to the deviation of charge transfer results. As displayed in Figure 4, when the collision energies are above 0.4 keV amu^{-1}, results of these two methods begin to deviate from each other with a difference of less than 8%.

Figure 5 displays some typical coupling matrix elements calculated by SCF and MCSCF. We can see that the coupling matrix elements between low-energy states are almost identical, e.g., $2^3\Sigma^+$-$4^3\Sigma^+$, but the differences between matrix elements calculated from these two methods increase with increasing orders of states. For instance, the differences of $2^3\Sigma^+$-$10^3\Sigma^+$ and $7^3\Sigma^+$-$8^3\Sigma^+$ are much more obvious than those of $2^3\Sigma^+$-$8^3\Sigma^+$. That is, the larger the sum of two states orders, the larger the difference in the coupling matrix elements calculated by SCF and MCSCF between them. As for the differences of cross sections below 0.01 keV amu^{-1} in these two methods, it should be ascribed to the sensitiveness for the finite-difference calculations in the low energy region.

Comparisons of the charge transfer cross sections between the present QMOCC and the available experimental and theoretical results are displayed in Figure 4. Theoretical predictions of charge transfer cross sections

below $0.065\,\mathrm{keV}\,\mathrm{amu}^{-1}$ are also given by present calculations. For the impact energies below $0.7\,\mathrm{keV}\,\mathrm{amu}^{-1}$, results of QMOCC are consistent with the measurements of Varghese et al. (1984) and calculations of Liu et al. (2016). For example at $E{\approx}0.6\,\mathrm{keV}\,\mathrm{amu}^{-1}$ the cross sections of Varghese et al. (1984) are about 7% larger than ours, but those of Aumayr & Winter (1985b) are around 20% smaller. In the energy range of 0.7–$2\,\mathrm{keV}\,\mathrm{amu}^{-1}$, the present charge transfer cross sections from both SCF and MCSCF are consistent with results of Liu et al. (2016) as well as measurements of Dubois & Toburen (1985) (the HG). Usually, the MCSCF calculation can provide better results than the SCF ones. However, the present results affirm that the differences in cross sections obtained from SCF and MCSCF orbital sets are less than 8%, since the correlation effect is not so important for the He^{+} colliding with Li. The results from MCSCF are closer to the AOCC data of Liu et al. (2016). As pointed out by Fritsch & Lin (1991), the AOCC method appears to be most suitable for the determination of coherence parameters in the intermediate-energy region (around $v/v_e \sim 1$ or dozens to hundreds of $\mathrm{keV}\,\mathrm{amu}^{-1}$). For the diffuse data of Dubois & Toburen (1985), more precise experiments are expected in this energy region. In addition, weak Stueckelberg oscillations like collisions between B^{4+} and H (Liu & Wang 2017) only appear in the present theoretical work, which can also be seen in the experimental measurements (Varghese et al. 1984; Aumayr & Winter 1985b; Dubois & Toburen 1985). The smaller measurements of Aumayr & Winter (1985b) may be the result of insufficient collection. The 15% smaller value of Bransden et al. (1984) than Liu et al. (2016) and the present QMOCC most probably results because of small expansion basis used in the calculation of Bransden et al. (1984).

The total QMOCC charge transfer cross sections for the singlet/triplet states in He^{+}-Li collisions are depicted in Figure 6 and compared with AOCC results of Liu et al. (2016). Our QMOCC data connect with the AOCC results smoothly around $0.1\,\mathrm{keV}\,\mathrm{amu}^{-1}$ and agree well with those of Liu et al. (2016) in the overlapping energy regions. Even the singlet and triplet states have similar potential energies and coupling matrix elements. In the low energy region, the cross sections are sensitive to the molecular structures. Different charge transfer cross sections will be lead by the tiny differences of molecular structures in the singlet and triplet manifolds (Liu & Wang 2017). It is clearly shown that the total charge transfer cross sections for the singlet states are obviously smaller than those for the triplet manifolds when energies are below $5\,\mathrm{keV}\,\mathrm{amu}^{-1}$. In addition, along with the increasing collision energies, the gap of cross sections between the
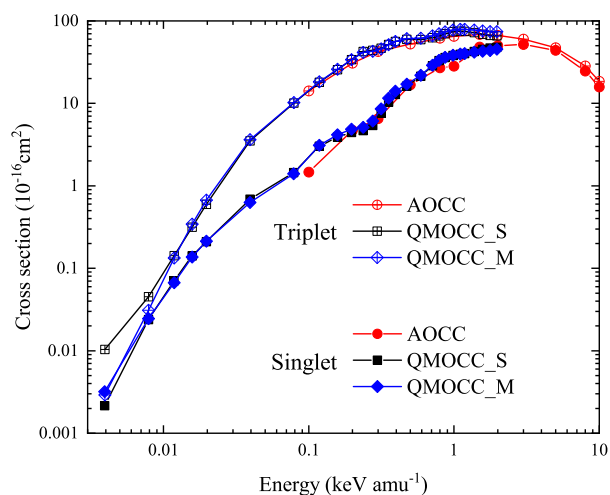
Fig. 6 Comparing examples of radial coupling matrix elements from SCF (*dash-dotted lines*) and MCSCF (*solid lines*) calculation.

singlet and triplet states increases firstly and subsequently decreases, with the turning point around $0.25\,\mathrm{keV}\,\mathrm{amu}^{-1}$. Firstly, from Figure 1 it is known that compared with the singlet states, the gaps of the initial channels [He^{+} + $\mathrm{Li}(1s^22s)$; $1^3\Sigma^+$] and its closest channel [$\mathrm{He}(1s2s)$ + Li^+; $2^3\Sigma^+$] for triplet states are much smaller in the large R range. Moreover, as displayed in Figure 2, in the large R range the radical couplings between [He^{+} + $\mathrm{Li}(1s^22s)$; $1^3\Sigma^+$] and [$\mathrm{He}(1s2s) + \mathrm{Li}^+$; $2^3\Sigma^+$] are slightly stronger than those between [He^{+} + $\mathrm{Li}(1s^22s)$; $2^1\Sigma^+$] and [$\mathrm{He}(1s2s) + \mathrm{Li}^+$; $3^1\Sigma^+$]. However, it is opposite for the internuclear distances near $3.0\,\mathrm{a.u.}$, which will have important contributions to cross sections at high collision energies. The different results of our QMOCC for SCF and MCSCF calculation will be explained in the state-selective cross sections part.

3.2.2 State-selective cross sections

In order to investigate the charge transfer cross sections in detail, the state-selective cross sections for electron captured to $\mathrm{He}(1s2l)$ and $\mathrm{He}(1s3l)$ are displayed in Figures 7 and 8 (Supplemental materials: Tables S2 and S3, see *http://www.raa-journal.org/docs/ Supp/ms4885SMaterials.pdf*), and are then compared with the only theoretical AOCC results of Liu et al. (2016). Our results are consistent with Liu et al. (2016) in the overlapping energy range. The electrons are dominantly captured to $\mathrm{He}(1s2l)$ from initial channels [He^{+} + $\mathrm{Li}(1s^22s)$; $2^1\Sigma^+/1^3\Sigma^+$] in our calculation due to small energy gaps and the long-range interactions of Demkov-type coupling between them. The cross sections of $3l$ are one order of magnitude smaller than those of $2l$,
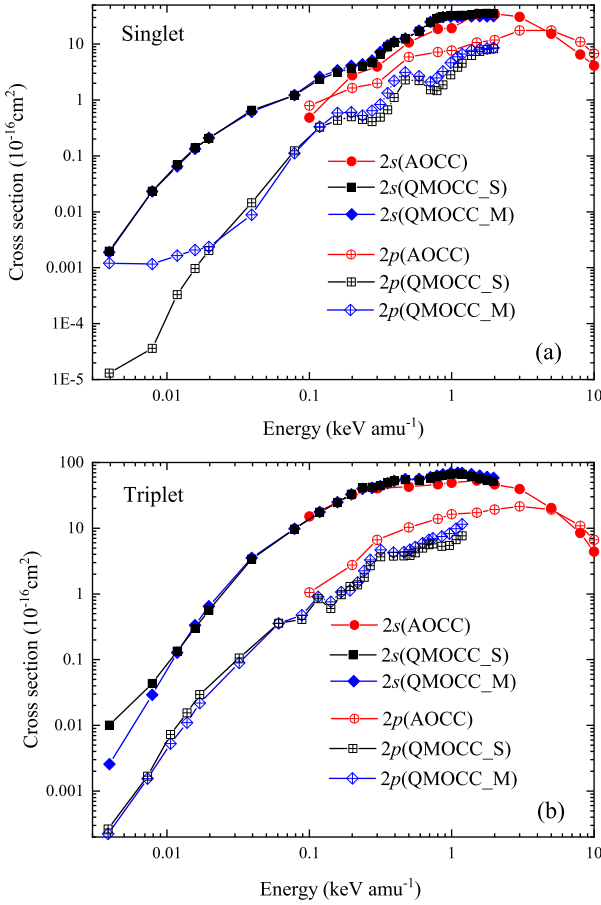
Fig. 7 State-selective cross sections for charge transfer to the singlet/triplet states of He $(1s2l)$ in He$^+$ colliding with Li and comparison with AOCC results of Liu et al. (2016).

Fig. 8 State-selective cross sections for charge transfer to the singlet/triplet states of He $(1s3l)$ in He$^+$ colliding with Li and comparison with AOCC results of Liu et al. (2016).

therefore only results of MCSCF calculation for $3l$ (labeled by QMOCC) are displayed in Figure 8.

When electrons are captured by the $2l$ states of He, the capture process to $2s$ $(2^3\Sigma^+)$ of triplet states is dominant because the $2^3\Sigma^+$ is the closest channel with the initial state. Moreover, the cross sections for He$(1s2s)$ $(3^1\Sigma^+)$ of singlet states and He$(1s2p)$ $(3^3\Sigma^+)$ of triplet states have close values due to the close energy gaps. Finally, the capture to the He$(1s2p)$ $(3^1\Sigma^+)$ is weakest for the largest energy defect in the $2l$ final states. Notably, the present QMOCC results of SCF and MCSCF calculation differ from each other below $0.02\,\mathrm{keV}\ \mathrm{amu}^{-1}$, e.g., capture to He$(1s2s)$ $(2^3\Sigma^+)$ and He$(1s2p)$ $(5^1\Sigma^+)$. As mentioned above, the cross sections are sensitive to the molecular structures in the low energy region. Although the curves of the SCF and MCSCF calculation for potential energy and radial coupling matrix elements between entrance and exit channels almost coincide with each other, the finite-difference calculations would lead to large differences in low energy regions. As for the electron captured to the $3l$ states of He, the cross sections of singlet/triplet states have

the same order of magnitude since they have similar energy gaps with initial channels.

3.3 Electron Collision Excitation

The adiabatic potential curves of charge transfer and excitation channels, as shown in Figure 1, appear alternately. Electrons can exchange among the capture states He$(1snl)$ + Li$^+(1s^2)$ and excitation states He$^+(1s)$ + Li$(1s2nl)$ through their couplings. Some couplings of those are especially strong, such as between [He$(1s2s)$ + Li$^+$; $3^1\Sigma^+$] and [He$^+$ + Li$(1s^22p)$; $4^1\Sigma^+$] states at about 3.5 a.u., and [He$(1s2p)$ + Li$^+$; $5^1\Sigma^+$] and [He$^+$ + Li$(1s^23s)$; $6^1\Sigma^+$] states ~ 7.0 a.u.. Some of those charge transfer and excitation states have long-range interactions and the potential energies are close, such as [He$(1s2p)$ + Li$^+$; $3^3\Sigma^+$] and [He$^+$ + Li$(1s^22p)$; $4^3\Sigma^+$] in triplet states, which can also lead to a certain amount of electron flux. Aumayr & Winter (1985a) measured emission cross sections of Li$(1s^22p)$Li$(1s^22s)$ formed from collisions of He$^+$ and Li in impact energies between 2 and $20\,\mathrm{keV}$
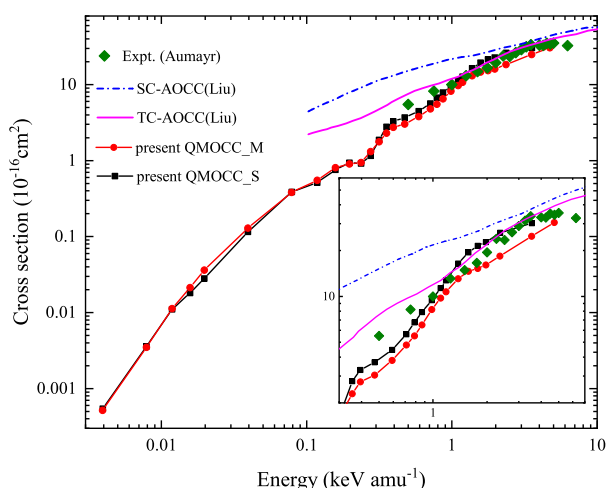
Fig. 9 Spin-averaged electron excitation cross sections of Li($1s^2 2p$) and comparison with other results. Theory: present QMOCC_M (*solid line with filled circles*) and QMOCC_S (*solid line with filled squares*) results, SC-AOCC (*dash-dotted line*) and TC-AOCC (*solid line*) results of Liu et al. (2016); experiment: emission cross section for the excitation of Li($1s2 2p$) (*filled diamonds*) by Aumayr & Winter (1985a).

(0.5–5 keV amu^{-1}). Liu et al. (2016) calculated the cross sections for electron excitation to the Li($1s^2 2p$) state by following the single- and two-center AOCC method (labeled by SC-AOCC and TC-AOCC) in the energy region of 0.1–100 keV amu^{-1}. The present QMOCC total cross sections for electron excitation to the Li($1s^2 2p$) atom together with the results of Aumayr & Winter (1985a) and Liu et al. (2016) are displayed in Figure 9 in the energy region of 0.003–3.5 keV amu^{-1}. The results of SCF and MCSCF calculations are also listed. Generally, our QMOCC calculations are in good mutual agreement in trend with the experimental data of Aumayr & Winter (1985a) and the TC-AOCC of Liu et al. (2016).

As the impact energies $E > 0.4$ keV amu^{-1}, our QMOCC Li($1s^2 2p$) excitation cross sections of SCF and MCSCF calculation also have differences, but the results of SCF calculation are slightly higher since the charge transfer cross sections of SCF are smaller than those of MCSCF. When the collision energies are below 1 keV amu^{-1}, the present calculations are smaller than those of Aumayr & Winter (1985a); this difference may result from the cascade contributions of Li($1s^2$nl, n>2) states on emission. The Li($1s^2 2p$) excitation cross sections from two-center AOCC calculations are smaller than those of single-center AOCC calculations, because the population of Li($1s^2$nl) states is also influenced by the intermediate charge-exchange couplings between He($1s$nl) and Li($1s^2$nl) states, which could reduce the population of electrons in the Li($1s^2 2p$) state in the collision evolution, particularly at low collision energies.
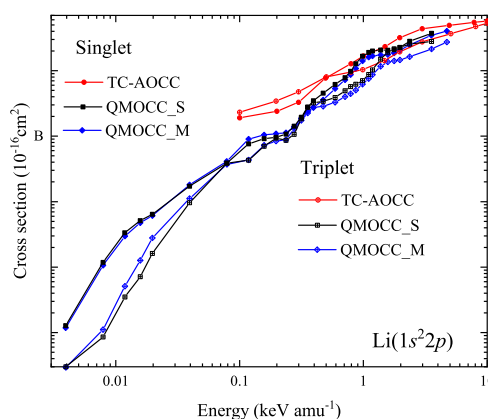
Fig. 10 State-selective cross sections of Li($1s^2 2p$) state in the singlet/triplet states and comparison with the two-center AOCC results of Liu et al. (2016).

When impact energies $E < 1$ keV amu^{-1}, our QMOCC electron excitation cross sections lie below the calculations of TC-AOCC from Liu et al. (2016), where the QMOCC methods are more reliable because of the limited validity of the AOCC method and the time is sufficient to perform the intermediate multi-step process for these energies (Liu et al. 2014).

The state-selective electron excitation cross sections for the Li($1s^2 2p$) state are featured in Figure 10 and compared with the TC-AOCC calculations of Liu et al. (2016). From Figure 10 it is notable that the difference in Li($1s^2 2p$) electron excitation between singlet and triplet s-tates is not as obvious as the corresponding charge transfer results, mainly due to their identical potential energies of [He$^+$ + Li($1s^2 2p$); $4^1\Sigma^+/4^3\Sigma^+$] in the asymptotic region. The reasons why the electron excitation cross sections for single states are larger than those of triplet states may result from these two cases. On the one hand, in comparison with the closest charge transfer channel [He($1s2p$)+Li$^+$; $3^3\Sigma^+$] of [He$^+$+Li($1s^2 2p$); $4^3\Sigma^+$], the [He($1s2s$)+Li$^+$; $3^1\Sigma^+$] are closer to initial state and their cross sections are larger, on the other hand, the [He($1s2s$)+Li$^+$; $3^1\Sigma^+$] and [He$^+$+Li($1s^2 2p$); $4^1\Sigma^+$] in single states have long-range interactions as displayed in Figure 2.

4 CONCLUSIONS

In the present article, the total and state-selective charge transfer and excitation cross sections for collisions of solar wind He$^+$ ions with Li atoms have been investigated by the QMOCC method in the energy range of 0.003 to 2 keV amu^{-1}. The different electronic structures calculated from SCF and MCSCF are used to describe the dynamical processes. On the whole, our QMOCC results are in good agreement with the experimental data of Varghese et al. (1984), Dubois & Toburen (1985) and theoretical results of Liu et al. (2016). Insufficient

collection and deficiencies in basis may have lead to the smaller results of Aumayr & Winter (1985b) and Bransden et al. (1984) (the LG). The total cross sections calculated from the SCF orbital sets are consistent with the MCSCF results within 8%. It can be considered that they have reached the convergence and the corresponding cross sections of He^+-Li collisions are reliable. The total charge transfer cross sections for the singlet manifolds are smaller than those of the triplet in low energy region due to the larger energy gaps between $He(1s2s)$ + $Li^+(1s^2)$ in singlet state and the initial state. The state-selective cross sections of present QMOCC are in accord with the AOCC results of Liu et al. (2016). In addition, the electron excitation processes of $Li(1s^22s)Li(1s^22p)$ agree well with $Li(1s^22p)$ emission cross sections of Aumayr & Winter (1985a) and AOCC results of Liu et al. (2016). Since the identical energy gaps between $Li(1s^22p)$ and the initial states for single and triplet states are in the asymptotic region, the difference between $Li(1s^22p)$ electron excitation cross sections in singlet/triplet states is not remarkable.

References

Auciello, O., Alonso, E. V., & Baragiola, R. A. 1976, Phys. Rev. A, 13, 985

Aumayr, F., & Winter, H. 1985a, Journal of Physics B Atomic Molecular Physics, 18, L741

Aumayr, F., & Winter, H. 1985b, Phys. Rev. A, 31, 67

Bacchus-Montabonel, M. C., & Ceyzeriat, P. 1998, Phys. Rev. A, 58, 1162

Bhardwaj, A., Elsner, R. F., Gladstone, G. R., et al. 2006, Journal of Geophysical Research (Space Physics), 111, A11225

Bhardwaj, A., Elsner, R. F., Randall Gladstone, G., et al. 2007, Planet. Space Sci., 55, 1135

Bransden, B. H., Ermolaev, A. M., & Shingal, R. 1984, Journal of Physics B Atomic Molecular Physics, 17, 4515

Bransden, B. H., & McDowell, M. R. C. 1992, Charge Exchange and the Theory of Ion-Atom Collision (Oxford: Clarendon Press), 300

Buenker, R. J., & Phillips, R. A. 1985, Journal of Molecular Structure: THEOCHEM, 123, 291

Cravens, T. E. 2000, ApJL, 532, L153

Dalgarno, A. 1985, Nuclear Instruments and Methods in Physics Research B, 9, 655

Dubois, R. D., & Toburen, L. H. 1985, Phys. Rev. A, 31, 3603

Dunning, Thom H., J. 1989, J. Chem. Phys., 90, 1007

Errea, L. F., Mendez, L., & Riera, A. 1982, Journal of Physics B Atomic Molecular Physics, 15, 101

Fritsch, W., & Lin, C. D. 1991, Phys. Rep., 202, 1

Gargaud, M., McCarroll, R., & Valiron, P. 1987, Journal of Physics B Atomic Molecular Physics, 20, 1555

Hans-Joachim, W., P., et al. 2010, Molpro: a Package of ab initio Programs

Heil, T. G., Butler, S. E., & Dalgarno, A. 1981, Phys. Rev. A, 23, 1100

Herrero, B., Cooper, I. L., & Dickinson, A. S. 1996, Journal of Physics B Atomic Molecular Physics, 29, 5583

Isler, R. C. 1994, Plasma Physics and Controlled Fusion, 36, 171

Johnson, B. R. 1973, Journal of Computational Physics, 13, 445

Kimura, M., & Lane, N. F. 1989, Advances in Atomic Molecular and Optical Physics, 26, 79

Kimura, M., & Lane, N. F. 1990, Phys. Rev. A, 41, 5938

Knowles, P. J., & Werner, H.-J. 1985, Chemical Physics Letters, 115, 259

Kramida, A., Ralchenko, Y., Reader, J., & Team, N. A. 2019, NIST Atomic Spectra Database (version 5.7.1)

Krasnopolsky, V. A., & Mumma, M. J. 2001, ApJ, 549, 629

Krebs, S., & Buenker, R. J. 1995, J. Chem. Phys., 103, 5613

Lin, X., Wu, Y., Wang, J. G., et al. 2019, A&A, 625, A29

Lischka, H., Nachtigallova, D., Aquino, A. J. A., et al. 2018, Chemical Reviews, 118, 7293

Liu, C. H., Liu, L., Qu, Y. Z., et al. 2010, Phys. Rev. A, 82, 022710

Liu, C.-H., & Wang, J.-G. 2017, European Physical Journal D, 71, 168

Liu, L., Li, X. Y., Wang, J. G., & Janev, R. K. 2014, Physics of Plasmas, 21, 062513

Liu, L., Wang, J. G., & Janev, R. K. 2016, Journal of Physics B Atomic Molecular Physics, 49, 105201

Lubinski, G., Juhász, Z., Morgenstern, R., & Hoekstra, R. 2001, Phys. Rev. Lett., 86, 616

McCullough, R. W., Goffe, T. V., Shah, M. B., et al. 1982, Journal of Physics B Atomic Molecular Physics, 15, 111

Polosukhina, N. S., & Shavrina, A. V. 2007, Astrophysics, 50, 381

Polosukhina, N., Shavrina, A., Drake, N., et al. 2010, Bulletin Crimean Astrophysical Observatory, 106, 57

Ramírez, I., Fish, J. R., Lambert, D. L., & Allende Prieto, C. 2012, ApJ, 756, 46

Schweinzer, J., Wutte, D., & Winter, H. P. 1994, Journal of Physics B Atomic Molecular Physics, 27, 137

Swaczyna, P., McComas, D. J., & Zirnstein, E. J. 2019, ApJ, 875, 36

Varghese, S. L., Waggoner, W., & Cocke, C. L. 1984, Phys. Rev. A, 29, 2453

Werner, H.-J., & Knowles, P. J. 1985, J. Chem. Phys., 82, 5053

Zygelman, B., Cooper, D. L., Ford, M. J., et al. 1992, Phys. Rev. A, 46, 3846